

An explainable hierarchical self attention-based approach for tremor detection in the time domain

Timothy Odonga¹, Jeanne M. Powell¹, Mark Saad², Richa Tripathi², Christine D. Esper², Stewart A. Factor², Hyeokhyen Kwon^{1,3‡}, J. Lucas Mckay^{1,2,3‡}

1 Department of Biomedical Informatics, School of Medicine, Emory University, Atlanta, GA, USA

2 Jean and Paul Amos Parkinson’s Disease and Movement Disorders Program, Department of Neurology, School of Medicine, Emory University, Atlanta, GA, USA

3 Wallace H. Coulter Department of Biomedical Engineering, Georgia Institute of Technology, Atlanta, GA, USA

‡These authors also contributed equally to this work.

✉Current Address: Department of Biomedical Informatics, School of Medicine, Emory University, Atlanta, GA, USA

¶Membership list can be found in the Acknowledgments section.

* lucas@dbmi.emory.edu

Abstract

Tremor is a common movement disorder associated with conditions like Parkinson’s disease and Essential tremor, traditionally diagnosed through expert clinician assessment. Current automated detection methods rely on frequency-domain features informed by clinical expertise. In this work, we present an explainable, two-stage hierarchical framework for tremor detection in the time domain that learns tremor patterns directly from 3D kinematic marker time-series data across entire tremor-provoking trials. Our framework combined a deep convolutional and long short-term memory network to learn tremor representations from short, discrete, non-overlapping time segments of kinematic time series data from trials, which are then processed by a vision transformer that models their long-term temporal dynamics of time segment features for trial (session) level classification. Evaluated across nine body parts, the framework achieved F1-scores of 0.594 – 0.947 depending on body parts (average: 0.765), falling short of the frequency-domain state-of-the-art performance (0.909) while requiring minimal preprocessing. Attention weights and gradient-based class activation maps (Grad-CAM) identified time-domain features of tremor across body parts. This proof of concept demonstrated the feasibility of data-driven time-domain modeling for tremor detection across anatomically diverse body parts, while reducing reliance on expert-engineered spectral features and providing posthoc interpretability of temporal and anatomical patterns of tremor.

Introduction

Tremor is an involuntary, rhythmic, oscillatory movement of a body part that occurs across a range of neurological conditions, including Parkinson’s disease (PD) and essential tremor (ET) [1–3]. Characterizing where, how, and under which conditions tremor appears is central to diagnosis and longitudinal assessment, yet in clinical practice, this characterization relies on expert observation by trained movement disorder

neurologists, creating a bottleneck in access and scalability. Consequently, there is strong motivation to automate tremor assessment from movement data [4–8].

Clinical assessment of tremor is formalized in clinical rating scales such as the Movement Disorder Society Unified Parkinson’s Disease Rating Scale Part III (MDS-UPDRS-III) [9] and The Essential Tremor Rating Scale (TETRAS) for ET [10]. In these assessments, patients perform standardized tasks designed to elicit tremor under specific conditions, including rest (e.g., when quietly sitting, during walking, and without voluntary activation), posture (e.g., hands held outstretched in front of the body), and action (e.g., alternately pointing from the examiner’s finger to the patient’s nose, among other tasks) [1,2]. Tremor is evaluated separately across body regions and task conditions, and clinicians assign ordinal severity scores based on visual observation, which reflect the maximum observed amplitude within a brief examination period [1]. Tremor constancy is scored separately from amplitude, reflecting the clinical recognition that tremor may be continuous or intermittent within a single trial and that this distinction carries diagnostic weight [9]. The conditions under which tremor appears, its distribution across body segments, and its temporal behavior within a trial are all clinically meaningful dimensions of assessment [1,2].

Automating this assessment requires reducing these multidimensional observations to computable features. Tremor frequency has historically served as the primary quantitative descriptor, alongside body distribution and provoking conditions [1,2], because it provides a relatively stable and easily measurable summary of the oscillatory process [1]. In PD, tremor typically occurs at a relatively narrow frequency band (roughly 4–6 Hz) and is thought to arise from a central oscillatory mechanism involving distributed basal ganglia–thalamo–cortical circuits [9]. ET similarly exhibits characteristic frequency bands (typically 4–12 Hz), though at higher frequencies than PD and primarily during posture [2]. Because this oscillation is relatively stable and narrow-band, frequency-based features (e.g., peak frequency, band power, and related spectral statistics) have been effective descriptors for identifying Parkinsonian tremor, and their clinical salience naturally motivated their adoption in automated detection pipelines [11–16].

Across sensing modalities including accelerometry [17], 3D optical kinematics [18] and pose recognition [19] among others [20], existing methods reflect this reliance on frequency representation. Prior work has typically framed tremor detection as a classification problem, in which motion signals are analyzed over short windows, transformed into the frequency domain, and reduced to descriptive statistics characterizing oscillatory content. These engineered features are then aggregated and used as inputs to classifiers that predict tremor presence or absence. This approach has proven effective for sustained, high-amplitude tremor, where spectral properties are relatively stable across a trial. However, it relies on an implicit stationary assumption [21,22] that does not hold for intermittent tremor (i.e., tremor that emerges, re-emerges, or fluctuates during a trial).

In clinical practice, expert neurologists are instructed to rate the worst tremor amplitude observed during a task, while constancy of tremor is scored separately on the MDS-UPDRS-III (e.g., rest tremor amplitude vs. constancy of rest tremor) [9]. However, automated methods that rely on aggregated spectral summaries average within-trial tremor variation over the entire recording, causing intermittent tremor to appear attenuated relative to the worst tremor amplitude. This can miss clinically meaningful fluctuations in tremor amplitude over time [8].

Furthermore, common steps in preprocessing pipelines can suppress physiologically meaningful temporal variation of tremor [8]. For example, clipping fixed intervals from the beginning or end of recordings to exclude artifacts and instability associated with the start of trials may remove segments that may contain intermittent tremor [23].

These pipelines also typically involve several sequential steps: zero-phase low-pass filtering for noise reduction, Savitzky-Golay derivative filtering for marker velocity calculation, Butterworth band-pass filtering for tremor frequency isolation, normalization for scaling, and spectral decomposition via Welch’s method or time-frequency decomposition via continuous wavelet transform for feature extraction [18,24,25]. Such cascaded operations also introduce cumulative latency [26], limiting applicability to real-time or continuous monitoring scenarios.

Existing tremor detection methods span traditional signal processing and modern deep learning approaches, yet consistently rely on frequency-domain representations. Traditional clinical algorithms predominantly convert kinematic data to the frequency domain via Fast Fourier Transform prior to tremor classification [18,20,27–29]. Wavelet-based methods occupy an intermediate position, decomposing signals into spectro-temporal components through continuous wavelet transforms or Kalman filtering frameworks [25,30,31], but most ultimately pass spectral image representations to classifiers [25,30]. Deep learning approaches, such as convolutional [32–34] and recurrent architectures [35–37] have been applied directly to tremor time series data, but these methods still predominantly rely on frequency-domain transformations or aggregate statistics as inputs [32,34]. No prior work has applied a hierarchical deep learning framework in the time domain to learn tremor-relevant representations directly from kinematic time series data for tremor detection.

In this work, we propose a two-stage hierarchical framework to address this gap. This work presents a proof-of-concept time-domain approach for tremor detection, offering a complementary method to existing frequency-domain pipelines. In the first stage, a deep learning model [38] learns tremor-relevant features from non-overlapping time segments of each trial directly from raw kinematic marker data, with minimal preprocessing. In the second stage, a classifier model aggregates the learned representations to produce a binary tremor-detection decision across the entire trial [39,40]. The framework also supports post-hoc interpretability, identifying which temporal windows and kinematic markers most influenced each detection [41,42].

Materials and methods

Dataset

Participants

Data were derived from recordings of 52 patients evaluated for movement disorders in the Brain Health 3D Motion Capture Laboratory at Emory University. All data were collected under approval of the Internal Review Board (IRB) at Emory University (IRB #00002688). Patients contributed one or more recording sessions corresponding to standardized tremor-provoking tasks.

Kinematic data acquisition

Participants were prompted to perform a standardized set of tremor-provoking tasks while instrumented with 60 reflective markers placed at predefined anatomical locations. Each contiguous recording corresponding to a single tremor-provoking task is referred to as a session. A detailed list and description of the tremor-provoking tasks are provided in Table 1. Kinematic data were captured using a 14-camera optical motion capture system (Motion Analysis Corporation, Rohnert Park, CA, USA) sampling at 120 Hz.

Table 1. Nomenclature and description of the tremor-provoking tasks implemented in the Saad dataset [18]

Code	Task
sit-rest	Seated with arms placed on the thighs
sit-arms-extended	Seated, with arms extended anteriorly and parallel to the floor
sit-UEopp	Seated, with arms in a “T” pose parallel to the ground with fingers at each hand opposed
sit-point	Seated, performing a finger-to-nose pointing task with the indicated extremity
sit-spiral	Seated, performing a spiral movement with the indicated extremity (right or left)
std-rest	Standing with arms at sides
std-arms-extended	Standing, with arms extended out parallel to the ground
std-UEopp	Standing, with arms in a “T” pose parallel to the ground with fingers of each hand opposed
walk-thru	Comfortable walking from one end to the other of the motion capture space

Clinical labeling of tremor

In parallel with kinematic acquisition, clinicians documented their observations of tremor in the patient’s clinical note (e.g., “mild, intermittent tremor in right hand”). These observations were converted into binary tremor labels (present vs absent) for each of 16 predefined body extremities (head, shoulders, thorax, pelvis, left/right hand, left/right foot, left/right proximal arm, left/right distal arm, left/right distal leg, and left/right proximal leg) and assigned at the session level. Only explicitly documented tremor present or absent observations were labeled; body parts not mentioned in the clinical note were treated as unlabeled to avoid assuming absence of tremor from lack of documentation.

Anatomical mapping for modeling

Multiple markers were part of a single extremity as illustrated in Figure S1. Detailed marker placement information for all body extremities is provided in Table S1, Table S2, and Table S3 reproduced from Saad *et al.* [18]. These tables document the anatomical descriptions and coding conventions for kinematic markers in each extremity.

Label distribution

Analyses were conducted on a subset of nine body extremities comprising both hands, both feet, the head, and four leg segments (left/right distal and proximal), totaling 1,750 recordings from all 52 subjects (77% of the full labeled dataset). The label distribution showed substantial class imbalance, with 714 tremor-present recordings (40.8%) versus 1,036 tremor-absent recordings (59.2%). Hand tremor dominated the subset (280 and 279 tremor-present recordings for the left and right hands, respectively), while head tremor was moderately represented (52 recordings). Leg and foot body extremities showed fewer tremor-present recordings, ranging from 8 to 30 recordings per extremity. Other body extremities (e.g., shoulder, pelvis) were excluded from the analysis as the number of tremor present recordings (≤ 5 recordings) was insufficient for

supervised training. The detailed distribution of tremor labels in the dataset is shown in Table S4 and has been described previously in Saad *et al.* [18].

Clinical baseline algorithm

At the Emory Brain Health 3D Motion Capture Laboratory, the current clinical standard for automated tremor detection relies on expert-engineered spectral features extracted from optical motion capture data, the gold standard for kinematic measurement. This approach comprises two complementary algorithms: a velocity-based method and an amplitude-based method. This approach is actively deployed for billable clinical assessments at the Emory Brain Health 3D Motion Capture Laboratory, where it has been iteratively refined over several years through real-world patient care workflows. Saad *et al.* [18] evaluated this method on the same dataset. For this study, we evaluated both algorithms and used the best-performing algorithm as the frequency-domain baseline.

The velocity-based algorithm applied zero-phase low-pass filtering (20 Hz) and Savitzky-Golay derivative filtering to displacement data to obtain smooth velocity estimates [24], computed power spectral densities using Welch’s method [43], and combined them via the Euclidean norm across the x, y, and z dimensions. Then, a log transformation and Savitzky-Golay smoothing were applied prior to peak detection [24]. Rule-based classification identified tremor via narrow, symmetric spectral peaks (bandwidth <2 Hz, center frequency <10 Hz), with features extracted independently per marker and aggregated using a winner-take-all approach that selected the marker with maximal tremor amplitude.

The amplitude-based algorithm applied 4th-order Butterworth high-pass filtering (2 Hz cutoff) to displacement data, computed single-sided frequency spectra via fast Fourier transform for each marker axis, and aggregated across all markers using a max operation to represent the most severe tremor at each frequency. Afterward, the aggregate spectrum underwent Savitzky-Golay smoothing before heuristic peak detection [24]. Rule-based classification identified tremor via peaks within the neurologic frequency range (3.5-10 Hz) that exceed an empirically determined amplitude threshold (0.1 mm), with aggregation performed in the frequency domain prior to peak selection rather than via winner-take-all marker selection. These spectral features were also evaluated with a Support Vector Machine (SVM) classifier using radial basis function kernels and 5-fold cross-validation [39].

Preprocessing

Session data were read from `.trc` files and transformed from world-centered to pelvis-anchored, body-centered coordinates using established kinematic mapping methods [44, 45]. Marker series in the global laboratory frame were translated to the pelvis center of mass, then rotated into the pelvis anatomical coordinate system using a rotation matrix constructed from anatomical markers (anterior superior iliac spine and sacrum), yielding right-anterior-vertical (R-A-V) coordinates that move with the pelvis segment. The transformed trajectories were then partitioned into non-overlapping four-second windows [46]. Windows shorter than four seconds were zero-padded to maintain uniform input dimensions. The four-second window duration was selected based on prior work demonstrating that brief motor events can be reliably detected within time windows of this length [47, 48]. Given that tremor labels were only provided at the session level in the Saad dataset, we applied the session-level label to each window within the session as a proxy label for supervised training.

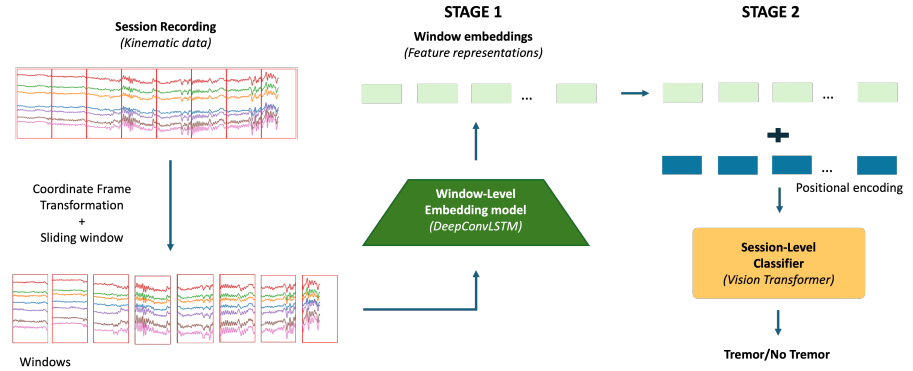


Fig 1. Overview of the two-stage hierarchical framework for tremor detection. A recording session of multi-channel kinematic marker data in world-centered coordinates is converted to body-centered coordinates and segmented into sliding windows. Each window is processed by a DeepConvLSTM to generate window-level embeddings, which are combined with positional encodings and passed to a Vision Transformer (ViT) for session-level tremor classification by modeling temporal dependencies across the full sequence of windows.

Hierarchical window-to-session modeling framework

Our training procedure followed a hierarchical, two-stage modeling framework designed to separate local tremor representation learning from session-level decision making.

1. A window-level model was trained to learn latent representations from fixed-length windows extracted from each recording session.
2. A session-level classifier was used to aggregate sequences of window-level embeddings produced in Stage 1 and generate a session-level tremor classification.

Figure 1 provides a visual overview of the two-stage training framework and the data flow from raw kinematic windows to session-level classification.

Window-level embedding model

The first stage learned fixed-dimensional representations of short-term tremor patterns from non-overlapping four-second windows. A deep convolutional and long short-term memory (DeepConvLSTM) architecture proposed by Ordonez and Roggen [38] was used to capture both local temporal features and short-range dependencies within each window. The model processed multivariate marker trajectories through four one-dimensional convolutional layers (64 kernels each), followed by two LSTM layers (128 units each). Convolutional layers extracted localized temporal patterns, while LSTM layers modeled their temporal evolution across the window. A fully connected output layer produced window-level predicted labels during training. After training, embeddings were extracted from the hidden state at the final timestep of the second LSTM layer, yielding a fixed 128-dimensional representation for each window that served as input to the session-level model.

Session-level classifier

The second stage aggregated window-level predicted labels to produce session-level tremor predicted labels. Three complementary approaches were evaluated, representing increasing levels of temporal modeling complexity.

First, a majority-vote approach assigned the session label based on the most frequent window-level predicted labels from the DeepConvLSTM model. This approach reflects a simple aggregation strategy analogous to summarizing the predominant tremor state observed during a task.

Second, an SVM classifier was trained using window-level embeddings aggregated by computing the mean values across each session. This method allowed the model to learn discriminative patterns across windows without explicitly modeling temporal order.

Third, a ViT encoder [40] was used to model temporal relationships among window embeddings. In this framework, window embeddings were treated as sequential tokens with positional encodings to preserve their order within the session. A learnable class token integrated information across all windows to generate a session-level prediction. Conceptually, this approach parallels clinical assessment, in which brief tremor episodes are interpreted in the context of the entire task.

Positional encodings were added to the embeddings passed to the ViT to preserve their temporal order, and a learnable class token was prepended to aggregate information across all windows into a single representation for classification [40, 41]. The token sequence was processed by a ViT encoder consisting of two transformer layers, each with multi-head self-attention (four heads, embedding dimension 128), followed by feed-forward networks. The final class token representation was passed to a fully connected classification head to generate the session-level tremor prediction.

Anatomical modeling configurations

To enable body-part-specific tremor detection, we trained separate models for each anatomical region rather than a single unified model. Each model was trained on data from a specific body part (e.g., hands, legs) across various tremor-provoking tasks. The input dimension of the window-level embedding model (DeepConvLSTM) was set to match the number of kinematic markers per extremity. Table S5 summarizes the number of kinematic markers in each body-part extremity.

Model performance and explainability

Performance evaluation

Model performance was evaluated using a five-fold user-independent nested cross-validation approach following the standard methods in machine learning (i.e., 80/20 train-test split ratio in each fold) [49, 50]. All data from each participant was assigned to a single fold, ensuring that no participant contributed data to both training and testing sets. This design enabled assessment of model generalization to previously unseen individuals. Within each training fold, data were further divided into training and validation sets, using an 80/20 split for model hyperparameter tuning.

Macro F1-score was selected as the primary evaluation metric to account for the class imbalance between tremor and no-tremor labels across body parts [51]. Precision and recall were also reported to characterize false-positive and false-negative detection behavior relevant to clinical interpretation. To account for stochastic variability in model training, five iterations of cross-validation were conducted using different random seeds, and the mean performance, with 95% confidence intervals, was reported.

Intermittent tremor subgroup analysis

To evaluate performance with respect to intermittent tremor, we conducted a targeted analysis of a subset of sessions from five participants who were clinically annotated as exhibiting intermittent tremor in the left hand, right hand, or left foot. These five

participants with 22 recordings were held out from training and used as a test set to evaluate model performance (using macro F1-score, precision, and recall) on intermittent tremor patterns. This subset represented cases in which tremor occurred sporadically rather than continuously throughout a task (see panel (a) of Figure S2).

Model explainability

Two complementary visualization approaches were applied to a high-performing iteration (complete 5-fold cross-validation run) to support the interpretation of model predictions. First, attention weights from the transformer were extracted to identify temporal windows that most influenced session-level classifications [41, 52, 53]. Attention scores from the class token were averaged across transformer layers and heads to produce a single importance value per window [41]. These scores were overlaid as color-coded window shading on time-series plots of per-marker displacement magnitudes, with red-bordered rectangles marking windows whose attention scores exceeded two standard deviations above the mean attention score (computed across all windows and sessions in the test fold), identifying windows most strongly prioritized by the model.

To quantify whether attention patterns differed between tremor present versus tremor absent recordings, we computed the variance of class-token attention scores across windows for each session. To account for repeated measures arising from multiple sessions per subject, session-level variances were aggregated to the subject level by taking the median variance across each subject’s correctly classified sessions within each class (tremor-present and tremor-absent separately). Only subjects with at least one correctly classified session in both the tremor-present and tremor-absent conditions were included, yielding a paired design. Sessions were pooled from folds with F1-score ≥ 0.80 to ensure that attention weights reflected meaningful learned representations. The paired distributions of subject-level median variance were compared using a one-tailed Wilcoxon signed-rank test (H_1 : tremor-present sessions exhibit greater window attention-score variance than tremor-absent sessions) [54].

Second, gradient-based class activation mapping (Grad-CAM) was applied to the final convolutional layer of the window-level model to identify marker channels contributing most strongly to tremor detection within individual windows [42]. This adaptation produced marker-level saliency maps indicating which kinematic features drove the model’s predictions.

Results

Performance across body parts

Performance varied across anatomical regions (F1-score: 0.594 – 0.947), as shown in Table 2. Head tremor detection achieved the highest performance, with the ViT session-level classifier reaching an F1-score of 0.947 ± 0.112 . Upper extremity tremor detection was also robust, with right-hand models achieving F1-scores 0.887 – 0.915 across all classifiers and left-hand models demonstrating moderate performance (F1: 0.816 – 0.844). Lower extremity detection showed greater variability. Proximal leg segments achieved relatively strong performance (F1 = 0.790), whereas distal foot tremor was most challenging, with both feet demonstrating the lowest performance (F1: 0.572 – 0.718). Classifier choice influenced performance differently across body parts. The ViT demonstrated the highest performance for head and left-hand tremor detection, whereas majority voting performed best for the right hand and several lower-extremity segments. Overall, selecting the best session-level classifier per body part yielded an average F1-score of 0.782 ± 0.071 across all body parts.

Table 2. Model performance for the tremor detection task for the body-part-specific model across different body parts. The window-level model used was DeepConvLSTM model [38]. Performance is reported as mean \pm 95% CI across five separate data folds. Non-overlapping confidence intervals indicate that the difference between the values is statistically significant ($p \leq 0.05$). N denotes the number of recordings with the number of subjects in parentheses. **Bold** text indicates which session-level classifier scored the highest performance per body part.

Body Part	N	Session-level Classifier	F1-score	Precision	Recall
L.Hand	517 (49)	Majority	0.832 \pm 0.200	0.831 \pm 0.198	0.843 \pm 0.208
		SVM	0.816 \pm 0.079	0.817 \pm 0.084	0.833 \pm 0.073
		ViT	0.844 \pm 0.154	0.849 \pm 0.198	0.845 \pm 0.073
R.Hand	521 (51)	Majority	0.915 \pm 0.182	0.921 \pm 0.174	0.921 \pm 0.159
		SVM	0.887 \pm 0.188	0.888 \pm 0.188	0.894 \pm 0.172
		ViT	0.892 \pm 0.180	0.895 \pm 0.182	0.889 \pm 0.176
Head	128 (24)	Majority	0.892 \pm 0.193	0.894 \pm 0.190	0.898 \pm 0.199
		SVM	0.898 \pm 0.230	0.904 \pm 0.221	0.896 \pm 0.233
		ViT	0.947 \pm 0.112	0.959 \pm 0.107	0.946 \pm 0.107
L.Foot	106 (17)	Majority	0.689 \pm 0.307	0.741 \pm 0.279	0.708 \pm 0.295
		SVM	0.682 \pm 0.303	0.725 \pm 0.292	0.690 \pm 0.298
		ViT	0.718 \pm 0.299	0.760 \pm 0.289	0.716 \pm 0.302
R.Foot	96 (17)	Majority	0.581 \pm 0.318	0.585 \pm 0.338	0.641 \pm 0.324
		SVM	0.572 \pm 0.322	0.559 \pm 0.336	0.607 \pm 0.310
		ViT	0.594 \pm 0.338	0.600 \pm 0.357	0.628 \pm 0.322
L.Dist.Leg	102 (22)	Majority	0.721 \pm 0.247	0.725 \pm 0.238	0.768 \pm 0.243
		SVM	0.679 \pm 0.254	0.686 \pm 0.258	0.721 \pm 0.247
		ViT	0.619 \pm 0.223	0.620 \pm 0.236	0.667 \pm 0.227
R.Dist.Leg	89 (22)	Majority	0.726 \pm 0.278	0.768 \pm 0.294	0.728 \pm 0.270
		SVM	0.725 \pm 0.286	0.767 \pm 0.296	0.719 \pm 0.281
		ViT	0.725 \pm 0.280	0.768 \pm 0.294	0.726 \pm 0.271
L.Prox.Leg	102 (22)	Majority	0.790 \pm 0.301	0.857 \pm 0.253	0.785 \pm 0.318
		SVM	0.771 \pm 0.337	0.846 \pm 0.284	0.759 \pm 0.362
		ViT	0.766 \pm 0.314	0.824 \pm 0.281	0.761 \pm 0.343
R.Prox.Leg	89 (22)	Majority	0.778 \pm 0.379	0.780 \pm 0.375	0.775 \pm 0.383
		SVM	0.780 \pm 0.374	0.786 \pm 0.366	0.778 \pm 0.380
		ViT	0.780 \pm 0.374	0.786 \pm 0.366	0.778 \pm 0.380
Average (all body parts)	-	Majority	0.769 \pm 0.068	0.789 \pm 0.067	0.785 \pm 0.059
		SVM	0.757 \pm 0.069	0.775 \pm 0.071	0.766 \pm 0.063
		ViT	0.765 \pm 0.077	0.785 \pm 0.077	0.773 \pm 0.068
		Best	0.782 \pm 0.071	0.803 \pm 0.071	0.791 \pm 0.066

Intermittent tremor subgroup analysis

Performance on intermittent tremor cases was lower than overall detection performance, with F1-scores ranging from 0.644 – 0.813 across body parts (Table 3). The majority

Table 3. Model performance for the tremor detection task for the body-part-specific model for patients annotated with intermittent tremor. The window-level model used is a DeepConvLSTM. Performance is reported as mean \pm 95% CI across five separate data folds. Non-overlapping confidence intervals indicate that the difference between the values is statistically significant ($p \leq 0.05$). N denotes the number of recordings with the number of subjects in parentheses. **Bold** text indicates which session-level classifier scored the highest performance per body part.

Body Part	N (recordings, subjects)	Session-level Classifier	F1-score	Precision	Recall
L.Hand	8 (3)	Majority	0.813 \pm 0.115	0.803 \pm 0.119	0.850 \pm 0.140
		SVM	0.794 \pm 0.141	0.787 \pm 0.150	0.849 \pm 0.167
		ViT	0.786 \pm 0.108	0.765 \pm 0.105	0.851 \pm 0.133
R.Hand	14 (5)	Majority	0.685 \pm 0.253	0.710 \pm 0.239	0.772 \pm 0.206
		SVM	0.651 \pm 0.251	0.663 \pm 0.183	0.755 \pm 0.223
		ViT	0.644 \pm 0.229	0.669 \pm 0.181	0.726 \pm 0.180
Hands	22 (5)	Majority	0.723 \pm 0.141	0.702 \pm 0.141	0.815 \pm 0.032
		SVM	0.698 \pm 0.140	0.678 \pm 0.124	0.805 \pm 0.040
		ViT	0.691 \pm 0.149	0.671 \pm 0.131	0.788 \pm 0.081

Table 4. Average model performance for the different tremor detection approaches. Performance is reported as mean \pm 95% CI across five separate data folds from the best-performing iteration. Non-overlapping confidence intervals indicate that the difference between the values is statistically significant ($p \leq 0.05$).

Approach	Feature Type	F1-score	Precision	Recall
Saad et al [18]	Frequency-domain	0.909 \pm 0.082	0.921 \pm 0.081	0.923 \pm 0.063
NeurDNet [55]	STFT	0.799 \pm 0.054	0.834 \pm 0.087	0.811 \pm 0.043
Our approach	Time-domain	0.782 \pm 0.071	0.803 \pm 0.071	0.791 \pm 0.066
WaveTremor [25]	Wavelet	0.758 \pm 0.105	0.797 \pm 0.091	0.763 \pm 0.109
Ensemble	Time-domain, STFT, Wavelet	0.837 \pm 0.056	0.845 \pm 0.067	0.851 \pm 0.047

voting classifier consistently achieved the highest performance in this subset, outperforming both SVM and ViT approaches. Detection accuracy varied substantially by anatomical region. The model demonstrated the strongest performance on the left hand, while the right hand showed lower accuracy and greater variability. When pooled across hands, the average F1-score was 0.704 (N=5 participants, 22 recordings) across all session-level classifiers, with majority voting achieving the best performance (0.723 \pm 0.141), followed by SVM (0.698 \pm 0.140) and ViT (0.691 \pm 0.149).

Model explainability

The ViT’s attention mechanism exhibited class-discriminative temporal focusing, concentrating on discrete windows of oscillatory activity in tremor-present sessions while distributing attention uniformly across windows in tremor-absent cases, as shown by the representative examples in Figure 2 of the sit spiral task performed on the left hand (Fold F1-score = 0.911). For the iteration from which the representative examples were

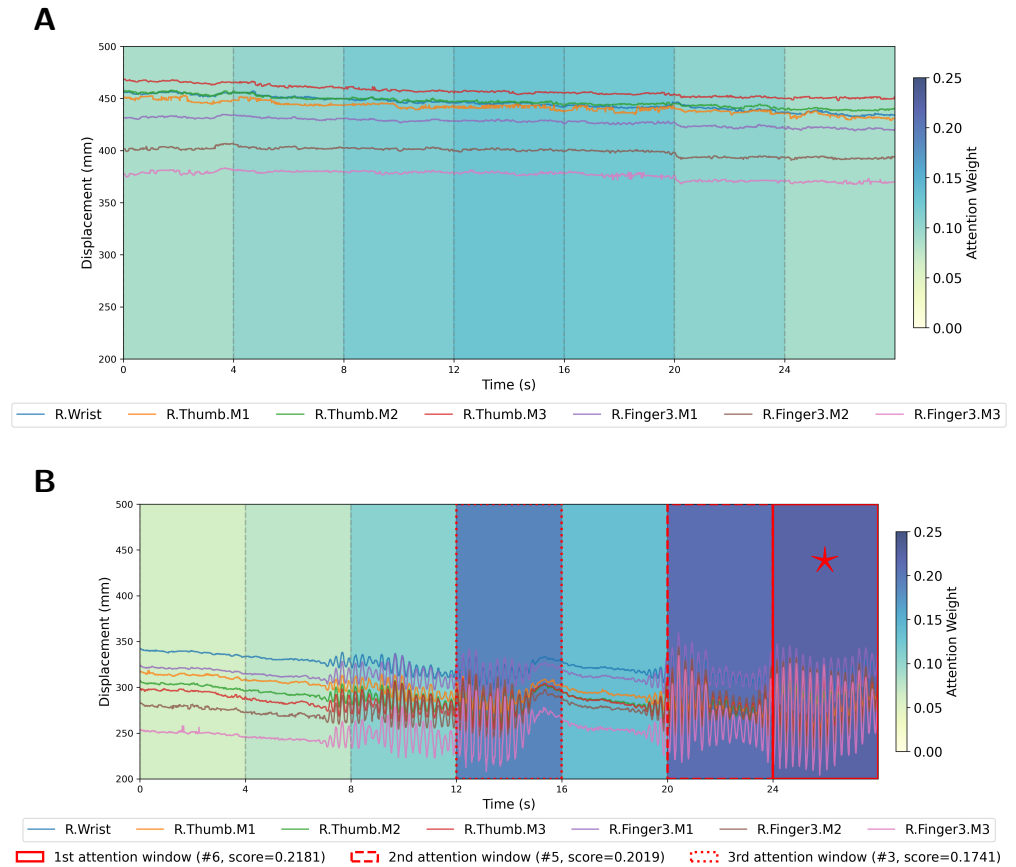


Fig 2. Visualization of attention weights and marker displacement time series for two correct model predictions during sit-spiral-left trials: (a) no tremor detected and (b) tremor detected. For correct tremor prediction, the red borders indicate the top-3 windows the model attends to (windows 4, 6, and 7). Red star: The ViT classifier assigns the highest attention weights to the seventh window (24–28 s), capturing the largest tremor amplitude. For the correct no-tremor prediction, the model assigns relatively uniform weights (approximately 0.05) across all windows, correctly identifying the absence of visible tremor patterns.

drawn, correctly classified tremor-present recordings exhibited significantly greater attention score variance than tremor-absent recordings ($W = 102$, $p < 0.001$, Wilcoxon signed rank test). Among misclassified sessions, no significant difference in attention variance was observed, suggesting that classification errors coincide with a failure of the attention mechanism to preferentially weight tremor-relevant windows.

Marker-level Grad-CAM visualizations (Figure 3) from the correctly classified tremor-present recording ((b) in Figure 2) localized tremor features to anatomically plausible regions. The saliency maps revealed concentrated importance on the distal thumb markers (i.e., R.Thumb.M2_R, R.Thumb.M1_V, R.Thumb.M1_A), with periodic burst activations reflecting the rhythmic oscillatory nature of tremor during the standing T-pose task. The model emphasized the right and vertical displacement components, consistent with maintaining the opposed-finger grip posture with arms extended parallel to the ground. In contrast, wrist markers (R.Wrist_V, R.Wrist_A, R.Wrist_R) and finger markers (R.Finger3.M3_V, R.Finger3.M2_V) showed minimal contribution, indicating that the model localized tremor features to the distal thumb markers, exhibiting the most pronounced oscillatory motion during the posture.

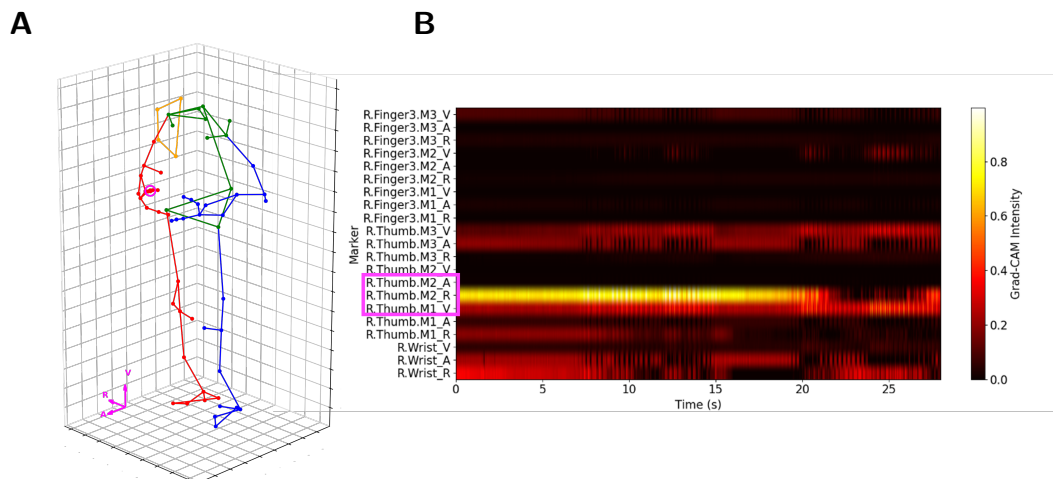


Fig 3. Marker-level interpretability for a correct hand tremor prediction (panel (B) in Figure 2). (A) 3D kinematic skeleton during a standing T-pose trial with opposed-finger grip, with the dominant markers highlighted with a circle. (B) Grad-CAM from the final convolutional layer of the window-level embedding model, localizing detection to the distal thumb markers (R.Thumb.M2, R.Thumb.M1), with emphasis on the right and vertical displacement components.

Feature representation comparison

To evaluate our choice of time-domain features, we compared them with frequency-based and time-frequency alternatives. We reimplemented the expert-derived frequency features from Saad *et al.* [18], refined through years of clinical use, and two time-frequency approaches: the wavelet-based method by Chen *et al.* [25] and the short-time Fourier transform (STFT) spectrogram-based CNN framework by Shahtalebi *et al.* [55]

Table 4 shows performance across the five approaches. The frequency-based method achieved the highest F1-score (0.909 ± 0.082), as expected, given that these features have been validated and refined through years of clinical practice. Our time-domain approach achieved 0.782 ± 0.071 without requiring domain-specific feature engineering. The two time-frequency approaches achieved 0.799 ± 0.054 for STFT spectrograms and 0.758 ± 0.105 for wavelets, with overlapping confidence intervals indicating no significant differences among the three learned approaches. Combining the three feature types (time-domain, STFT, and Wavelet) in an ensemble improved performance to 0.837 ± 0.056 , narrowing the gap with the frequency-based method (clinical baseline), with overlapping confidence intervals indicating no statistically significant difference. Despite performing below the clinical baseline, all learned approaches had confidence intervals that overlapped with those of the frequency-based method.

Discussion

Primary findings

This work presented a data-driven hierarchical framework for tremor detection in the time domain that learned directly from raw kinematic marker data with minimal preprocessing (i.e., global-to-egocentric coordinate transformation and sliding window segmentation) and without relying on expert-driven spectral features. The two-stage approach, combining DeepConvLSTM for window-level feature extraction with ViT for session-level classification, achieved an average F1 Score of 0.765 across nine body parts

and tremor-provoking tasks. Attention-weight visualizations provided interpretable explanations of which temporal segments influenced tremor predicted labels, addressing transparency concerns in clinical machine learning applications. These findings provided proof of concept for data-driven deep learning approaches to tremor detection, demonstrating their feasibility as an alternative to methods relying on expert driven features and preprocessing pipelines [8].

Our hierarchical deep learning framework achieved strong tremor detection performance for clinically critical body parts, with head tremor reaching $F1 = 0.947$ and hand tremor achieving $F1 = 0.844 - 0.915$. Performance varied substantially across the nine body parts evaluated, including bilateral hands, feet, head, and leg segments, with the lower extremities proving more challenging ($F1 = 0.594-0.790$) due to subtle tremor manifestations and complex biomechanical patterns during different tremor-provoking tasks. This difference in performance between the upper and lower extremities reflects the clinical reality that tremor occurrence and manifestation vary across body parts, with upper-body tremor providing more robust signals for detection [56]. Notably, the optimal session-level classifier architecture varied by body part: ViT achieved superior performance on the head and feet, while simple majority voting outperformed more complex classifiers across several leg segments. This variation likely reflects substantial class imbalance across body parts, ranging from balanced cases in the hands to highly imbalanced cases in the distal and proximal legs (Table S4), and suggests that aggregation strategies should be matched to the temporal characteristics of tremor in specific anatomical regions.

Comparison with prior work

Our time-domain approach achieved an average F1-score of 0.765 across nine body parts, significantly lower than 0.909 for the frequency-domain methods implemented in Saad *et al.* [18] ($p < 0.01$, Wilcoxon signed rank test), but comparable to time-frequency approaches: 0.799 for the STFT spectrogram-based method [55]. and 0.758 for the wavelet-based approach [25], with no significant differences among the three learned methods. While overall performance was lower than that of expert-engineered frequency features, our framework offers important trade-offs: it requires substantially less preprocessing and clinical-domain input, and learns tremor representations directly from raw kinematic signals rather than from engineered frequency features. The performance gap reflected the efficiency of expert-driven feature engineering, which directly encodes clinical knowledge about tremor characteristics, whereas data-driven approaches require larger datasets and more extensive training to learn comparable representations from raw signals [8, 57, 58]. Our explainability analysis also provided complementary insights: while frequency-domain SHAP (SHapley Additive exPlanations) identifies the frequency at which tremor occurs [18, 59], our attention mechanisms and Grad-CAM reveal when tremor emerges (temporal windows) and which kinematic markers contribute to its detection [41, 42]. The comparable performance between our time-domain approach and the wavelet-based approach suggests that wavelet decomposition offered a limited advantage over direct temporal modeling for tremor detection across body parts, though both learned methods fell short of expert-engineered features.

Intermittent tremor subgroup analysis

Intermittent tremor proved substantially more challenging to detect, with F1-scores decreasing by 0.1-0.2 points across body parts. This performance gap likely reflects both the inherent difficulty of detecting intermittent tremor episodes and the limitations of session-level proxy labeling, which may have introduced label noise, as many windows may have inherited tremor labels even when they contain no actual

tremor activity. Notably, simple majority voting consistently outperformed ViT in these cases, suggesting that learning temporal dependencies via attention may be sensitive to label noise, whereas aggregating independent window predicted labels is more robust. Furthermore, transformer-type models are data-hungry and require large amounts of training data to achieve strong performance [60, 61], and the limited number of intermittent tremor sessions ($N=5$ participants, 22 recordings) may have constrained ViT’s ability to learn meaningful temporal dependencies in this subgroup. Fine-grained temporal annotations, such as window-level tremor labels or onset and offset timestamps within sessions, would address the labeling limitation and potentially improve the detection of these clinically relevant edge cases.

Clinical implications

The time-domain approach achieved performance within 10% of the frequency-domain clinical baseline algorithm despite data imbalance across extremities, suggesting potential as a complementary method to standard frequency-domain approaches in clinical workflows. Modeling temporal patterns with explainability at both the marker level (via Grad-CAM) and the temporal level (via attention weights) may offer additional clinical utility in differentiating tremor types, such as PD from ET [62]. This temporal and spatial resolution could supplement current clinical workflows, enabling structured documentation of when tremor occurred during a session and which body parts were most affected, thereby complementing clinicians’ notes.

Limitations and future work

Our evaluation was restricted to a single dataset from one clinical center [18], limiting the generalizability of our findings across patient populations, motion capture systems, and clinical settings. Future work should validate this approach on multi-site datasets with diverse patient populations and acquisition protocols to establish the robustness of time-domain deep learning for tremor detection.

The presence of substantial label imbalance with some body parts severely constrained performance for anatomical locations where tremor rarely manifests. The right foot achieved the lowest F1-score of 0.594 with substantially fewer tremor-positive training sessions compared to the head and hands. This reflected the clinical reality that tremor prevalence varies across body parts, but it also revealed a fundamental challenge in applying supervised learning to such problems. Future work may explore data augmentation [63], semi-supervised learning [64], or transfer learning from high-prevalence to low-prevalence body parts to improve model performance in underrepresented anatomical regions [65].

Our evaluation on intermittent tremor detection was constrained by only five subjects with hand recordings, making it difficult to draw robust conclusions from this subgroup. Future work will prioritize collecting larger cohorts of patients with intermittent tremor to enable more robust evaluation of the framework’s performance on this clinically relevant subpopulation.

Coarse session-level labels provide no information on when tremor occurred in a session. Our proxy-labeling of tremor during window-level training assigned the same label to all windows within a session, even though tremor may occur in only a subset of those windows. Fine-grained temporal annotations that mark the exact onset and offset of tremor would provide more accurate supervision and potentially improve the detection of low-amplitude, intermittent episodes.

Formulating tremor detection as a binary classification problem (i.e., present versus absent) in a session discards rich clinical information that could enhance diagnostic utility. Clinicians assess severity, frequency, characteristics, amplitude fluctuations, and

contextual factors, while our framework reduces this multidimensional evaluation to a single binary decision [1,9]. Future work will extend the framework to multi-class severity classification using conformal prediction, thereby providing clinicians with both severity-class predictions and statistically valid uncertainty bounds [66].

Conclusion

Tremor is a common movement disorder associated with conditions like PD and ET, traditionally diagnosed through expert clinician assessment. Current automated tremor detection methods predominantly rely on frequency-domain or time-frequency representations, leaving a methodological gap for pure time-domain temporal modeling approaches that could better capture tremor variability. This work presents a proof-of-concept hierarchical framework for time-domain tremor detection that learns directly from raw kinematic data without requiring expert feature engineering. Our approach achieved F1-scores of 0.765 across nine body parts, comparable to time-frequency methods (0.799 for STFT spectrograms, 0.758 for wavelets) but lower than frequency-domain methods (0.909) refined through decades of clinical use. By modeling temporal dynamics through window-level feature extraction and session-level sequence modeling, our approach captured tremor patterns across nine body parts and provided dual explainability through attention weights (identifying important temporal windows) and GradCAM (identifying critical kinematic markers). Our results demonstrate that temporal modeling could offer a complementary alternative to frequency-domain approaches by preserving information about when and where tremor occurs. Given the limitations of the lack of window-level labels and data imbalance across body parts, these results suggest that temporal approaches with window-level annotations and sufficient data could match frequency-domain performance. Future work incorporating fine-grained temporal annotations could bridge the remaining performance gap relative to expert-engineered features while preserving the benefits of data-driven temporal representation learning, thereby advancing automated tremor assessment.

References

1. Bhatia KP, Bain P, Bajaj N, Elble RJ, Hallett M, Louis ED, et al. Consensus Statement on the classification of tremors. from the task force on tremor of the International Parkinson and Movement Disorder Society. *Movement disorders*. 2018;33(1):75-87.
2. Deuschl G, Bain P, Brin M. Consensus statement of the Movement Disorder Society on Tremor. Ad Hoc Scientific Committee. *Movement Disorders*. 1998;13(Suppl 3):2-23. doi:10.1002/mds.870131303.
3. Testa CM, Haubenberger D, Patel M, Caughman CY, Factor SA. Tremor in Medicine and Other Secondary Tremors. In: *Tremors*. Oxford University Press; 2022. p. 75-84. Available from: <https://doi.org/10.1093/med/9780197529652.003.0007>. doi:10.1093/med/9780197529652.003.0007.
4. Pulliam CL, Heldman DA, Brokaw EB, Mera TO, Mari ZK, Burack MA. Continuous assessment of levodopa response in Parkinson's disease using wearable motion sensors. *IEEE Transactions on Biomedical Engineering*. 2017;65(1):159-64.

5. Heldman DA, Espay AJ, LeWitt PA, Giuffrida JP. Clinician versus machine: reliability and responsiveness of motor endpoints in Parkinson's disease. *Parkinsonism & related disorders*. 2014;20(6):590-5.
6. Dorsey ER, Bloem BR. The Parkinson pandemic—a call to action. *JAMA neurology*. 2018;75(1):9-10.
7. Maetzler W, Klucken J, Horne M. A clinical view on the development of technology-based tools in managing Parkinson's disease. *Movement Disorders*. 2016;31(9):1263-71.
8. De A, Bhatia KP, Volkmann J, Peach R, Schreglmann SR. Machine Learning in Tremor Analysis: Critique and Directions. *Movement Disorders*. 2023;38(5):717-31. doi:10.1002/mds.29376.
9. Goetz CG, Tilley BC, Shaftman SR, Stebbins GT, Fahn S, Martinez-Martin P, et al. Movement Disorder Society-sponsored revision of the Unified Parkinson's Disease Rating Scale (MDS-UPDRS): scale presentation and clinimetric testing results. *Movement disorders: official journal of the Movement Disorder Society*. 2008;23(15):2129-70.
10. Elble RJ. The essential tremor rating assessment scale. *Journal of Neurology & Neuromedicine*. 2016;1(4).
11. Samadi E, Ahmadi H, Rahatabad FN. Analysis of hand tremor in parkinson's disease: Frequency domain approach. *Frontiers in Biomedical Technologies*. 2020.
12. Beuter A, Edwards R. Using Frequency Domain Characteristics to Discriminate Physiologic and Parkinsonian Tremors. *Journal of Clinical Neurophysiology*. 1999 9;16(5):484. Available from: <http://dx.doi.org/10.1097/00004691-199909000-00010>. doi:10.1097/00004691-199909000-00010.
13. Pang Y, Christenson J, Jiang F, Lei T, Rhoades R, Kern D, et al. Automatic detection and quantification of hand movements toward development of an objective assessment of tremor and bradykinesia in Parkinson's disease. *Journal of Neuroscience Methods*. 2020 3;333:108576. Available from: <http://dx.doi.org/10.1016/j.jneumeth.2019.108576>. doi:10.1016/j.jneumeth.2019.108576.
14. Lukšys D, Jonaitis G, Griškevičius J. Quantitative Analysis of Parkinsonian Tremor in a Clinical Setting Using Inertial Measurement Units. *Parkinson's Disease*. 2018 jun 21;2018:1-7. Available from: <http://dx.doi.org/10.1155/2018/1683831>. doi:10.1155/2018/1683831.
15. Brittain JS, Cagnan H, Mehta AR, Saifee TA, Edwards MJ, Brown P. Distinguishing the Central Drive to Tremor in Parkinson's Disease and Essential Tremor. *The Journal of Neuroscience*. 2015 jan 14;35(2):795-806. Available from: <http://dx.doi.org/10.1523/JNEUROSCI.3768-14.2015>.
16. Meigal AY, Rissanen SM, Tarvainen MP, Georgiadis SD, Karjalainen PA, Airaksinen O, et al. Linear and nonlinear tremor acceleration characteristics in patients with Parkinson's disease. *Physiological Measurement*. 2012 feb 28;33(3):395-412. Available from: <http://dx.doi.org/10.1088/0967-3334/33/3/395>. doi:10.1088/0967-3334/33/3/395.

17. Zeuner KE, Shoge RO, Goldstein SR, Dambrosia JM, Hallett M. Accelerometry to distinguish psychogenic from essential or parkinsonian tremor. *Neurology*. 2003;61(4):548-50. doi:10.1212/01.wnl.0000076183.34915.cd.
18. Mark Saad, Hefner S, Donovan S, Bernhard D, Tripathi R, Factor SA, et al. Development of a Tremor Detection Algorithm for Use in an Academic Movement Disorders Center. *Sensors*. 2024;24(15):4960. doi:10.3390/s24154960.
19. Friedrich MU, Roenn AJ, Palmisano C, Alty J, Paschen S, Deuschl G, et al. Validation and application of computer vision algorithms for video-based tremor analysis. *npj Digital Medicine*. 2024;7:165. doi:10.1038/s41746-024-01153-1.
20. Haubenberger D, Abbruzzese G, Bain P, Bajaj N, Benito-León J, Bhatia K, et al. Transducer-Based Evaluation of Tremor. *Movement Disorders*. 2016;31(9):1327-36. doi:10.1002/mds.26649.
21. Brown RG, Hwang PYC. *Introduction to Random Signals and Applied Kalman Filtering: With MATLAB Exercises and Solutions*. 3rd ed. Wiley; 1997.
22. Yates RD, Goodman DJ. *Probability and Stochastic Processes: A Friendly Introduction for Electrical and Computer Engineers*. 4th ed. John Wiley & Sons; 2025.
23. Jeon H, Lee W, Park H, Lee HJ, Kim SK, Kim HB, et al. High-accuracy automatic classification of Parkinsonian tremor severity using machine learning method. *Physiological measurement*. 2017;38(11):1980.
24. Gallagher NB. Savitzky-golay smoothing and differentiation filter. *Eigenvector Research Incorporated*. 2020.
25. Chen X, Koltermann K, Clapham J, Blackwell G, Cloud L, Pretzer-Aboff I, et al. WaveTremor: Tremor Detection for Parkinson's Disease via Spatial-Temporal Learning. In: *Proceedings of the ACM/IEEE International Conference on Connected Health: Applications, Systems and Engineering Technologies*; 2025. p. 309-13.
26. Oppenheim AV. *Discrete-time signal processing*. Pearson Education India; 1999.
27. Raethjen J, Lauk M, Köster B, Fietzek U, Friege L, Timmer J, et al. Tremor analysis in two normal cohorts. *Clinical Neurophysiology*. 2004;115(9):2151-6.
28. Deuschl G, Lauk M, Timmer J. Tremor classification and tremor time series analysis. *Chaos: An Interdisciplinary Journal of Nonlinear Science*. 1995;5(1):48-51.
29. Timmer J, Lauk M, Häußler S, Radt V, Köster B, Hellwig B, et al. Cross-spectral analysis of tremor time series. *international Journal of Bifurcation and chaos*. 2000;10(11):2595-610.
30. Jung W, Koltermann K, Helm N, Blackwell G, Pretzer-Aboff I, Cloud L, et al. IMU Sensing Data-Based Kinetic Tremor Detection in Parkinson's Disease Patients. In: *Proceedings of the 20th ACM Conference on Embedded Networked Sensor Systems*; 2022. p. 772-3.
31. Shahtalebi S, Atashzar SF, Patel RV, Mohammadi A. WAKE: Wavelet decomposition coupled with adaptive Kalman filtering for pathological tremor extraction. *Biomedical Signal Processing and Control*. 2019;48:179-88.

32. Kim HB, Lee WW, Kim A, Lee HJ, Park HY, Jeon HS, et al. Wrist sensor-based tremor severity quantification in Parkinson's disease using convolutional neural network. *Computers in biology and medicine*. 2018;95:140-6.
33. Sigcha L, Pavón I, Costa N, Costa S, Gago M, Arezes P, et al. Automatic resting tremor assessment in Parkinson's disease using smartwatches and multitask convolutional neural networks. *Sensors*. 2021;21(1):291.
34. San-Segundo R, Zhang A, Cebulla A, Panev S, Tabor G, Stebbins K, et al. Parkinson's disease tremor detection in the wild using wearable accelerometers. *Sensors*. 2020;20(20):5817.
35. Ribeiro LC, Afonso LC, Papa JP. Bag of samplings for computer-assisted Parkinson's disease diagnosis based on recurrent neural networks. *Computers in biology and medicine*. 2019;115:103477.
36. Hssayeni MD, Jimenez-Shahed J, Burack MA, Ghoraani B. Wearable Sensors for Estimation of Parkinsonian Tremor Severity during Free Body Movements. *Sensors*. 2019;19(19). Available from: <https://www.mdpi.com/1424-8220/19/19/4215>. doi:10.3390/s19194215.
37. Shahtalebi S, Atashzar SF, Samotus O, Patel RV, Jog MS, Mohammadi A. PHTNet: Characterization and deep mining of involuntary pathological hand tremor using recurrent neural network models. *Scientific reports*. 2020;10(1):2195.
38. Ordóñez FJ, Roggen D. Deep Convolutional and LSTM Recurrent Neural Networks for Multimodal Wearable Activity Recognition. *Sensors*. 2016;16(1):115. Available from: <https://www.mdpi.com/1424-8220/16/1/115>. doi:10.3390/s16010115.
39. Suthaharan S. Support vector machine. In: *Machine learning models and algorithms for big data classification: thinking with examples for effective learning*. Springer; 2016. p. 207-35.
40. Dosovitskiy A. An image is worth 16x16 words: Transformers for image recognition at scale. *arXiv preprint arXiv:201011929*. 2020.
41. Vaswani A, Shazeer N, Parmar N, Uszkoreit J, Jones L, Gomez AN, et al. Attention is all you need. *Advances in neural information processing systems*. 2017;30.
42. Selvaraju RR, Cogswell M, Das A, Vedantam R, Parikh D, Batra D. Grad-cam: Visual explanations from deep networks via gradient-based localization. In: *Proceedings of the IEEE international conference on computer vision*; 2017. p. 618-26.
43. Welch P. The use of fast Fourier transform for the estimation of power spectra: A method based on time averaging over short, modified periodograms. *IEEE Transactions on audio and electroacoustics*. 1967;15(2):70-3.
44. Cappozzo A, Catani F, Della Croce U, Leardini A. Position and orientation in space of bones during movement: anatomical frame definition and determination. *Clinical biomechanics*. 1995;10(4):171-8.
45. Pham MH, Elshehabi M, Haertner L, Heger T, Hobert MA, Faber GS, et al. Algorithm for turning detection and analysis validated under home-like conditions in patients with Parkinson's disease and older adults using a 6 degree-of-freedom inertial measurement unit at the lower back. *Frontiers in neurology*. 2017;8:135.

46. Bulling A, Blanke U, Schiele B. A Tutorial on Human Activity Recognition Using Body-Worn Inertial Sensors. *ACM Computing Surveys*. 2014 January;46(3):1-33. doi:10.1145/2499621.
47. Bächlin M, Plotnik M, Roggen D, Maidan I, Hausdorff JM, Giladi N, et al. Wearable Assistant for Parkinsons Disease Patients with the Freezing of Gait Symptom. *IEEE Transactions on Information Technology in Biomedicine*. 2010 March;14(2):436-46. doi:10.1109/TITB.2009.2036165.
48. Kwon H, Clifford GD, Genias I, Bernhard D, Esper CD, Factor SA, et al. An Explainable Spatial-Temporal Graphical Convolutional Network to Score Freezing of Gait in Parkinsonian Patients. *Sensors*. 2023 February;23(4). doi:10.3390/s23041766.
49. Wainer J, Cawley G. Nested cross-validation when selecting classifiers is overzealous for most practical applications. *Expert Systems with Applications*. 2021;182:115222.
50. Parvande S, Yeh HW, Paulus MP, McKinney BA. Consensus features nested cross-validation. *Bioinformatics*. 2020;36(10):3093-8.
51. Opitz J, Burst S. Macro F1 and Macro F1. *CoRR*. 2021;abs/1911.03347. Available from: <https://arxiv.org/abs/1911.03347>. arXiv:1911.03347. doi:10.48550/arXiv.1911.03347.
52. Xu K, Ba J, Kiros R, Cho K, Courville A, Salakhudinov R, et al. Show, Attend and Tell: Neural Image Caption Generation with Visual Attention. In: Bach F, Blei D, editors. *Proceedings of the 32nd International Conference on Machine Learning*. vol. 37 of *Proceedings of Machine Learning Research*. Lille, France: PMLR; 2015. p. 2048-57. Available from: <https://proceedings.mlr.press/v37/xuc15.html>.
53. Carion N, Massa F, Synnaeve G, Usunier N, Kirillov A, Zagoruyko S. End-to-end object detection with transformers. In: *European conference on computer vision*. Springer; 2020. p. 213-29.
54. Wilcoxon F. Individual comparisons by ranking methods. In: *Breakthroughs in statistics: Methodology and distribution*. Springer; 1992. p. 196-202.
55. Shahtalebi S, Atashzar SF, Patel RV, Jog MS, Mohammadi A. A deep explainable artificial intelligent framework for neurological disorders discrimination. *Scientific reports*. 2021;11(1):9630.
56. Mahendran S, Bichsel O, Gassert R, Baumann CR, Imbach LL, Waldvogel D. Differentiation of Parkinson's disease tremor and essential tremor based on a novel hand posture. *Clinical Parkinsonism & Related Disorders*. 2022;7:100146.
57. Esteva A, Robicquet A, Ramsundar B, Kuleshov V, DePristo M, Chou K, et al. A guide to deep learning in healthcare. *Nature medicine*. 2019;25(1):24-9.
58. Rajkomar A, Oren E, Chen K, Dai AM, Hajaj N, Hardt M, et al. Scalable and accurate deep learning with electronic health records. *NPJ digital medicine*. 2018;1(1):18.
59. Lundberg SM, Lee SI. A unified approach to interpreting model predictions. In: *Proceedings of the 31st International Conference on Neural Information Processing Systems*. NIPS'17. Red Hook, NY, USA: Curran Associates Inc.; 2017. p. 4768-4777.

60. Liu Y, Sangineto E, Bi W, Sebe N, Lepri B, Nadai M. Efficient training of visual transformers with small datasets. *Advances in Neural Information Processing Systems*. 2021;34:23818-30.
61. Wen Q, Zhou T, Zhang C, Chen W, Ma Z, Yan J, et al. Transformers in time series: A survey. *arXiv preprint arXiv:220207125*. 2022.
62. Thanawattano C, Pongthornseri R, Anan C, Dumnin S, Bhidayasiri R. Temporal fluctuations of tremor signals from inertial sensor: a preliminary study in differentiating Parkinson's disease from essential tremor. *Biomedical engineering online*. 2015;14(1):101.
63. De B, Sakevych M, Metsis V. The Impact of Data Augmentation on Time Series Classification Models: An In-Depth Study with Biomedical Data. In: *International Conference on Artificial Intelligence in Medicine*. Springer; 2024. p. 192-203.
64. Huynh T, Nibali A, He Z. Semi-supervised learning for medical image classification using imbalanced training data. *Computer methods and programs in biomedicine*. 2022;216:106628.
65. Gupta P, Malhotra P, Narwariya J, Vig L, Shroff G. Transfer learning for clinical time series analysis using deep neural networks. *Journal of Healthcare Informatics Research*. 2020;4(2):112-37.
66. Angelopoulos AN, Bates S. Conformal prediction: A gentle introduction. *Foundations and Trends in Machine Learning*. 2023;16(4):494-591.

Acknowledgments

Supporting information



Fig S1. This figure illustrates marker placement and motion capture facility as described in Saad *et al.* [18]. **(A)** Figure illustrating the marker placement on the 16 body extremities of a study participant. **(B)** De-identified “wire frame” representation of the participant in **(A)**. **(C)** The origin of the kinematic coordinate system is superimposed in the clinical motion capture facility.

Table S1. Kinematic marker descriptions for markers on the trunk. Markers that appear on both sides of the body are listed for the right side only and are coded beginning with "R". Replacing this character with "L" will designate the corresponding marker on the left side of the body.

Extremity	Marker Code	Description
Head	Front_Head	Center of forehead, on cap
	JAW	Mental protuberance
	RBHD	Right back head, on cap
	RFHD	Right front head, on cap
	Rear_Head	Rear of head, on cap
	TopHead	Top of head
	Top_Head	Top of head
Shoulders	C7	Seventh cervical vertebra
	RBAK	Right scapula (asymmetry marker)
	RSHO	Right acromioclavicular joint
	R.Shoulder	Right acromion process
	STRN	Xiphoid process
Pelvis	LASI	Left anterior superior iliac spine
	RASI	Right anterior superior iliac spine
	RIC	Right iliac crest
	RPSI	Right posterior superior iliac spine
	R.ASIS	Right anterior superior iliac spine
	V_Sacral	Sacrum
Thorax	CLAV	Clavicular notch
	R.Clavicle	Right clavicle
	R.Scap_Inf	Right scapula inferior angle
	R.Scapula	Right supraspinous fossa
	T10	10th thoracic vertebra

Table S2. Kinematic marker descriptions for markers on the arms. Markers that appear on both sides of the body are listed for the right side only and are coded beginning with "R". Replacing this character with "L" will designate the corresponding marker on the left side of the body.

Extremity	Marker Code	Description
R_Dist_Arm	RFRM	Lateral surface of forearm
	RWRA	Radial side of wrist
	RWRB	Ulnar side of wrist
	R_Forearm	Lateral surface of forearm
	R_Radius	Right styloid process of radius
	R_Ulna	Mid region of ulna
R_Hand	RFIN	Third finger, first metacarpal joint
	RFINGM2	Third finger, second metacarpal joint
	RFINGM3	Third finger, most distal segment
	RTHM1	Thumb, first metacarpal
	RTHM2	Thumb, second metacarpal
	RTHM3	Thumb, most distal segment
	R_Finger3_M1	Third finger, first metacarpal joint
	R_Finger3_M2	Third finger, second metacarpal joint
	R_Finger3_M3	Third finger, most distal segment
	R_Hand	Radial surface of wrist
	R_Thumb_M1	Thumb, first metacarpal
	R_Thumb_M2	Thumb, second metacarpal
R_Thumb_M3	Thumb, most distal segment	
R_Wrist	Radial surface of wrist	
R_Prox_Arm	RELB	Right lateral epicondyle
	R_BicepsLateral	Lateral surface of upper arm
	R_Biceps_Lateral	Lateral surface of upper arm
	R_Elbow	Right lateral epicondyle
	R_Elbow_Medial	Right medial epicondyle

Table S3. Kinematic marker descriptions for markers on the legs. Markers that appear on both sides of the body are listed for the right side only and are coded beginning with "R". Replacing this character with "L" will designate the corresponding marker on the left side of the body.

Extremity	Marker Code	Description
R_Dist_Leg	RANK	Lateral aspect of ankle
	RANKM	Medial aspect of ankle
	RTIB	Midpoint of tibia
	R_Ankle	Lateral aspect of ankle
	R_Ankle_Medial	Medial aspect of ankle
	R_Shank	Midpoint of tibia
R_Foot	RFTM	Dorsal/medial surface of foot midway between ankle and toe
	RHEE	Distal surface of heel
	RTOE	Third metatarsal
	R_Hallux	Dorsal surface of big toe
	R_Heel	Distal surface of heel
	R_MedFoot	Dorsal/medial surface of foot midway between ankle and toe
R_Prox_Leg	R_Toe	Third metatarsal
	RKNE	Lateral aspect of flexion–extension axis of knee
	RKNEM	Medial aspect of flexion–extension axis of knee
	RTHI	Upper lateral 1/3 surface of thigh
	R_Knee	Lateral aspect of flexion–extension axis of knee
	R_Knee_Medial	Medial aspect of flexion–extension axis of knee

Table S4. Frequency distribution of tremor labels for each body part extremity in the Saad dataset [18]. L refers to Left, R refers to Right.

Body Part	Absent	Present
Head	76	52
Shoulders	71	1
Thorax	78	1
Pelvis	71	1
L_Dist_Arm	73	5
R_Dist_Arm	72	1
L_Hand	237	280
R_Hand	242	279
L_Prox_Arm	71	3
R_Prox_Arm	72	1
L_Dist_Leg	81	21
R_Dist_Leg	8	8
L_Foot	76	30
R_Foot	81	15
L_Prox_Leg	81	21
R_Prox_Leg	81	8

Table S5. The number of kinematic markers in each extremity in the Saad dataset [18]. L refers to Left, R refers to Right.

Body Part	Number of Markers
Head	12
Shoulders	9
Thorax	15
Pelvis	9
L_Dist_Arm	9
R_Dist_Arm	9
L_Hand	21
R_Hand	21
L_Prox_Arm	9
R_Prox_Arm	9
L_Dist_Leg	9
R_Dist_Leg	9
L_Foot	9
R_Foot	9
L_Prox_Leg	9
R_Prox_Leg	9

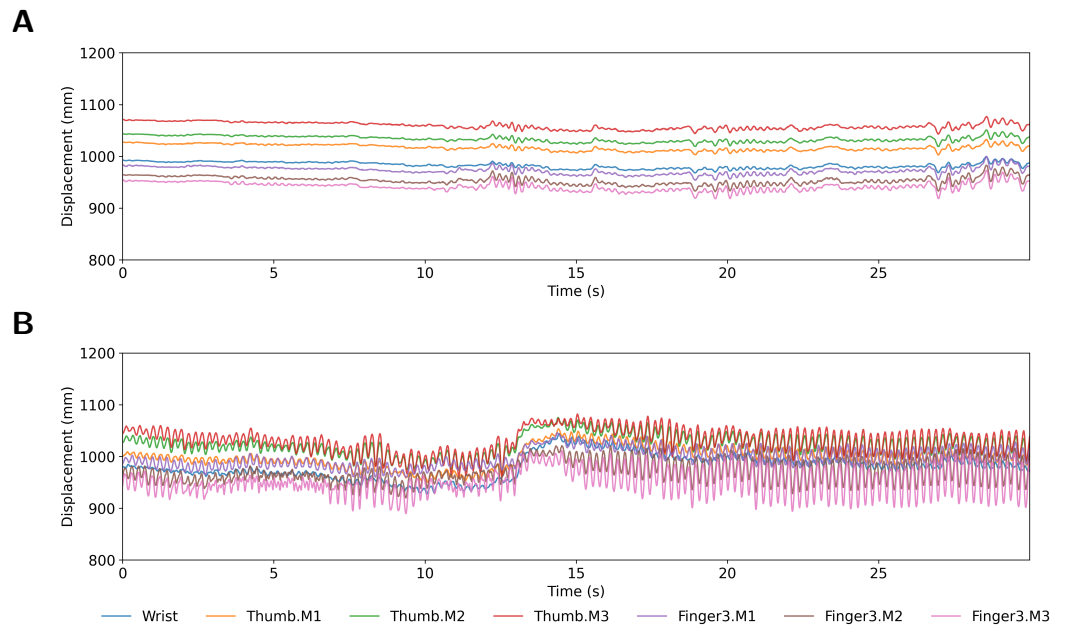


Fig S2. Intermittent versus sustained tremor during the sit-UEopp task (seated with arms in a T-pose parallel to the ground, fingers opposed). The raw clinician annotations were “*littler intermittent*” for the intermittent example (A) and “*significant*” for the sustained example (B). In (A), tremor patterns are observed during short time periods during the trial, i.e., 12–14 s, 18–22 s, and 26–28 s. In (B), tremor patterns are observed throughout the session.